NONLINEAR FREQUENCY-MODULATED INFRARED THERMAL WAVE DETECTION OF DEBONDING DEFECTS IN CFRP LAMINATES

by

Qing-Ju TANG [a,*], ***Si-Jie AN*** [a], ***Cui-Zhu FENG*** [a], ***Chi-Wu BU*** [b]

[a] School of Mechanical Engineering, Heilongjiang University of Science and Technology, Harbin 150022, China

[b] College of Light Industry, Harbin University of Commerce, Harbin 150028, China

NLFM infrared thermal wave detection system was established to detect and analyze debonding defects of different sizes of CFRP laminates. Principal component analysis, thermal signal reconstruction and total harmonic distortion are used to process the infrared image sequence collected by thermal imager, and the processing effect is evaluated by signal-to-noise ratio. Compared with the other two image sequence processing algorithms, PCA has better effect, can effectively improve the signal-to-noise ratio, and the defect edge in the processed image is clearer.

Key words: *CFRP;Infrared thermal imaging; NLFM; PCA; TSR; THD*

Introduction

CFRP is widely used in aerospace, automobile industry, petroleum industry and ship industry because of its excellent heat resistance, low thermal expansion coefficient [1, 2] and high specific strength. During the preparation and service process of CFRP laminates, due to the influence of manufacturing process, cyclic stress and impact damage, it is easy to form defects such as interlayer delamination, surface scratches, matrix cracks and debonding [3]. These defects seriously affect the performance of CFRP. Therefore, it is necessary to use non-destructive testing technology to detect CFRP defects.

Active infrared thermal wave nondestructive testing technology is to apply controllable thermal excitation to the detected object, collect surface temperature data by infrared thermal imager, analyze and process the collected infrared image sequence, so as to realize the rapid detection of internal defects of materials. According to the type of excitation source, infrared thermal wave detection methods are classified into pulse method [4,5], phase-locked method [6], linear frequency modulation method [7], nonlinear frequency modulation method and two-phase coding method [8].

Nonlinear frequency modulation (NLFM) infrared thermal wave detection is a new non-destructive testing method that uses nonlinear frequency modulation signal modulation excitation to detect specimen defects. Compared with the traditional linear frequency modulation (LFM) infrared thermal wave detection, the signal can obtain lower sidelobes without weighting processing, which can effectively improve the image SNR. The NLFM signal used in this paper is obtained by

* Corresponding author; e-mail: tangqingju@126.com

logarithmic frequency modulation. Because the frequency of thermal excitation applied to the surface of the specimen is logarithmic, it can effectively solve the problem of poor detection effect of pulse method and phase-locked method on different depths and different types of defects [9].

In this paper, the debonding defects of CFRP laminates with different diameter and depth are detected and analyzed by using nonlinear frequency modulation infrared thermal wave detection method, and the infrared image sequences collected by thermal imager are processed by principal component analysis (PCA). Finally, the debonding defects of CFRP laminates are detected successfully.

Detection principle and test system construction

The NLFM infrared thermal wave detection system is built, as shown in Figure 1. The peak power of a single halogen lamp is 1000W, the infrared thermal imager model is FLIR A655SC, the pixel resolution is 640 pixels × 480 pixels, and the data acquisition card model is NI-USB6259BNC. The principle is that the data acquisition card collects NLFM excitation signal sent by the computer and sends the collected signal to the dimmer, which controls the halogen lamp to emit energy light wave to generate temperature difference on the surface of CFRP laminates. Finally, the infrared thermal imager is used to collect surface temperature data of CFRP laminates and sends it to the computer. Data analysis software is used to process the collected data and finally achieve the purpose of identifying defects. If the heat flow is composed of static component and dynamic component, the heat flow excitation formula of nonlinear frequency modulation (logarithmic frequency modulation) reads [10]

$$q(t)=q_{\mathrm{S}}+q_{\mathrm{D}}=\frac{q_{\max}}{2}\left\{1+\cos\left[2\pi\left(\frac{T}{\ln\left(\frac{f_e}{f_s}\right)}\left(f_s\left(\frac{f_e}{f_s}\right)^{\frac{t}{T}}-f_s\right)\right)+\varphi_0\right]\right\},t\in[0,T] \tag{1}$$

where $q(t)$ is the surface heat flux density, $q_{\max}$ is the peak of surface heat flux density, q_{S} is the static component of surface heat flow, q_{D} is the surface heat flow component, T is the modulation time of NLFM modulation signal, f_e is the termination frequency, f_s is the initial frequency, and φ_0 is the initial phase.

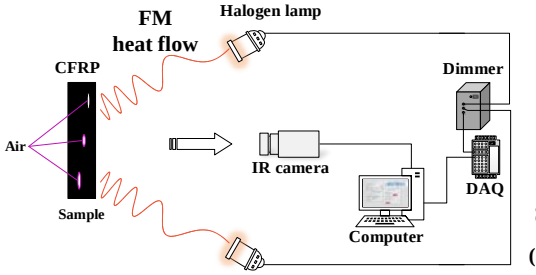

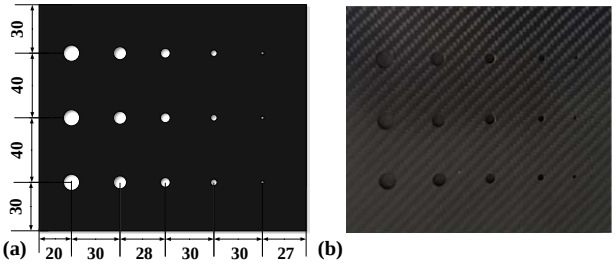

Figure 1. Infrared Thermal Wave Testing System **Figure 2. Diagram of CFRP laminates**

Test

Specimen preparation

In order to study the ability of NLFM infrared thermal wave nondestructive testing technology to detect debonding defects of CFRP laminates with different diameters and depths, CFRP laminate specimens are designed as shown in Figure 2.

Test parameters

The halogen lamp power was set to 2000 W, the initial frequency of NLFM signal was set to 1 Hz, the termination frequency was set to 0.06 Hz, and the modulation time was set to 13 seconds to apply heat flow excitation to the specimen. Set the sampling frequency of the thermal imager to 20Hz and the sampling time to 20 seconds to collect the surface temperature of CFRP laminates.

Test results and analysis

NLFM heat flow excitation is applied to the CFRP laminate specimen to obtain the original heat map at different times.

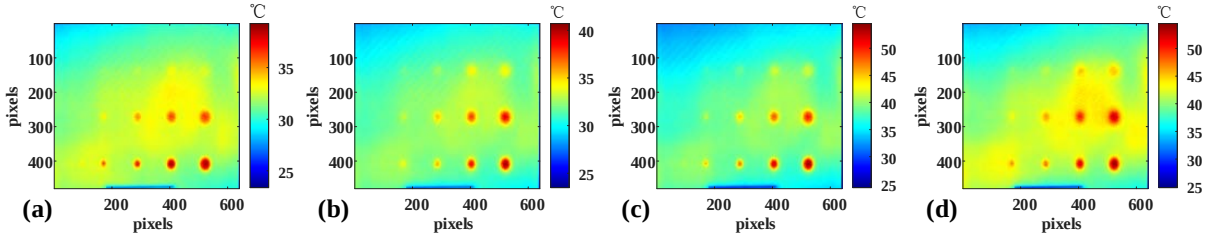

Figure 3. Original heat maps at different times; (a) 5seconds, (b) 10seconds, (c) 15seconds, and (d) 20seconds

It can be seen from Figure 3 that after the heat flow excitation is applied to the surface of the CFRP laminate specimen, the defect is detected at 5 seconds, but the defect detection with a depth of 1.5 mm is more blurred. At the 10th second, the defect at 1.5mm was gradually detected, and the defect detection results at 15 seconds were more obvious than before. The 20th second began to appear transverse thermal diffusion, defect detection showed fuzzy.

Figure 4 shows the influence of debonding defects of different diameths and depths on surface temperature difference of CFRP laminates. Figure 4(a) shows that for debonding defects of the same depth, the larger the diameter is, the more heat accumulated at the debonding defects due to heat insulation will be, and the temperature difference will be more obvious. It can be seen from Figure 4(b) that in the case of the same defect diameter, the shallower the distance from the excitation surface of the debonding defect location, the larger the temperature difference will be.

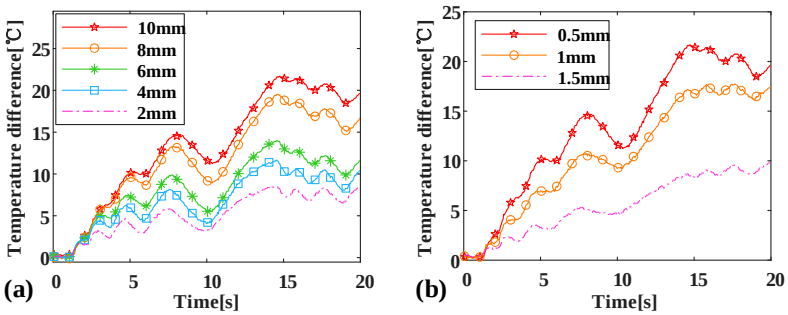

Figure 4. Influence of debonding defects of different sizes on surface temperature; (a) different diameters (b) different depths

The test data were normalized

In order to ensure that subsequent different image sequence processing algorithms can be

compared in the same order of magnitude, all test data are normalized. Here, we present

$$G = \frac{G_0 - G_{\min}}{G_{\max} - G_{\min}} \tag{2}$$

where G is the normalized test data, G_0 is the original test data, $G_{\max}$ is the maximum of the original test data, and $G_{\min}$ is the minimum of the original test data.

Image sequence processing

Thermal Signal Reconstruction (TSR)

TSR is a polynomial fitting process in the logarithmic domain for the selected infrared image sequence to optimize the image quality and improve the defect contrast. The TSR modeling process [11] is as follows.

First, the difference between the temperature of the excitation surface after heating and the initial temperature before heating ($\Delta T_{surf}(t)$) is expressed as follows

$$\Delta T_{surf}(t) = \frac{q_0}{e\sqrt{\pi t}} \tag{3}$$

Transform the temperature difference $\Delta T_{surf}(t)$ into the logarithmic domain reads

$$\ln(\Delta T_{surf}(t)) = \ln(\frac{q_0}{e}) - \frac{1}{2}\ln(\pi n) \tag{4}$$

The logarithmic domain change of temperature response of a single pixel point can be expressed by n-order polynomial fitting as follows

$$\ln(\Delta T_{surf}(t)) = \sum_{n=0}^{N} a_n [\ln(t)]^n \tag{5}$$

On the basis of logarithmic domain, the first and second derivative are respectively taken to obtain images of low-order coefficients and high-order coefficients. This implies that

$$\Delta T_{surf}(t) = \exp(\sum_{n=0}^{N} a_n [\ln(t)]^n) \tag{6}$$

$$\frac{d\Delta T_{surf}(t)}{dt} = \exp(\sum_{n=0}^{N} n a_n [\ln(t)]^{n-1}) \tag{7}$$

$$\frac{d^2\Delta T_{surf}(t)}{dt^2} = \exp(\sum_{n=0}^{N} n(n-1) a_n [\ln(t)]^{n-1}) \tag{8}$$

where q_0 is the energy absorbed by the surface, e is the thermal emissivity of the material, and t is the time.

The results after TSR processing are shown in Figure 5. Figure 5(a) is the logarithmic fitting result of polynomial, Figure 5(b) is the logarithmic fitting result of first-order differential polynomial, and Figure 5(c) is the logarithmic fitting result of second-order differential polynomial. Through comparison, it can be seen that the second-order differential improves the contrast of infrared images and more defects can be detected, but some defect-free areas appear noise, resulting in blurred edges of detected defect images.

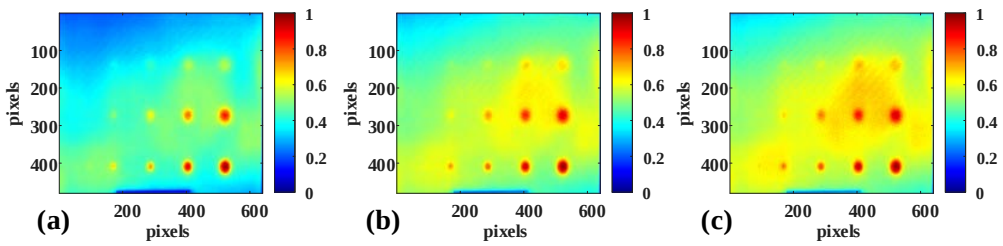

Figure 5. TSR processing result graph; (a) logarithmic fitting, (b) first-order differentiation, and (c) second-order differentiation

Principal Component Analysis (PCA)

In 2002, Rajic[12] proposed that PCA could be used to filter part of noise signals and extract image features. There are two methods to solve principal components in principal component analysis, one is eigenvalue decomposition covariance matrix, the other is SVD decomposition covariance matrix. SVD decomposition covariance matrix is used to solve the principal components. Generally, A frame of infrared heat map can be represented by an $I \times J$ matrix C_k, that is to say,

$$C_k = \begin{bmatrix} a_{11} & \cdots & a_{1j} \\ \vdots & \ddots & \vdots \\ a_{i1} & \cdots & a_{ij} \end{bmatrix}, \quad k = 1,2,3,...,n \tag{9}$$

where k is the number of frames in the infrared image sequence.

If PCA algorithm is applied to infrared heat map data, 3D infrared heat map matrix representing time and space changes must be transformed into 2D matrix D, as shown in Figure 6.The covariance matrix E is obtained by normalization of matrix D, and its eigenvalues are obtained by SVD decomposition of matrix E, i.e.,

$$E = URV^T \tag{10}$$

where, U is the eigenvector matrix of dimension $P \times Q$, R is the diagonal matrix of $Q \times Q$, where elements greater than or equal to zero represent the singular value of matrix E, and V^T is the transpose of matrix $Q \times Q$. The eigenvector matrix U was transformed into the inverse process of vectorization, and the image matrix F_m of each principal component was obtained by SVD decomposition, namely,

$$F_m = \begin{bmatrix} a_{11} & \cdots & a_{1j} \\ \vdots & \ddots & \vdots \\ a_{i1} & \cdots & a_{ij} \end{bmatrix}, \quad m = 1,2,3,...,n \tag{11}$$

where m is the corresponding principal component number.

The first principal component obtained from principal component analysis is shown in Figure6. It can be seen from Figure6(a) that PCA algorithm has good noise reduction ability, and the noise caused by twill noise on the surface of some CFRP laminates and transverse thermal diffusion of defects is removed, and the defect edge is more obvious.

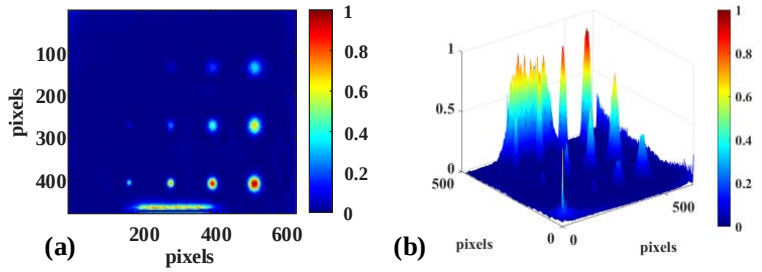

Figure 6. Results of principal component analysis; (a) 2-D diagram, (b) 3-D diagram

Total Harmonic Distortion (THD)

THD adopts the idea of microelectronics. Because the system is not completely linear, the output signal has an extra Harmonic component than the input signal, resulting in signal Distortion [13]. Therefore, THD algorithm is used to quantify the amount of harmonic distortion or noise in the signal.

THD_P can be defined as

$$THD_P = \frac{\sum_{n=2}^{\infty} P_n}{P_1} = \frac{\sum_{n=2}^{\infty} V_n^2}{V_1^2} \tag{12}$$

Another way to get the total harmonic distortion using amplitude ratio is defined as

$$THD_A = \frac{\sqrt{\sum_{n=2}^{\infty} V_n^2}}{V_1} \tag{13}$$

In order to apply total harmonic distortion to infrared thermal imaging, Equation (3) is transformed into Laplace transform to obtain the frequency response relation of defect-free region under ideal state, that is to say,

$$F_{Peak} = F(s) = \frac{q_0}{e\sqrt{\pi}} \cdot \frac{\Theta(z,s)}{\sqrt{s}} \tag{14}$$

where, P_n is the power of the NTH harmonic, F_{Peak} is the voltage of the NTH harmonic, and $\Theta(z,s)$ is the Laplace transform of the temperature $T(z,t)$ perpendicular to the excitation surface.

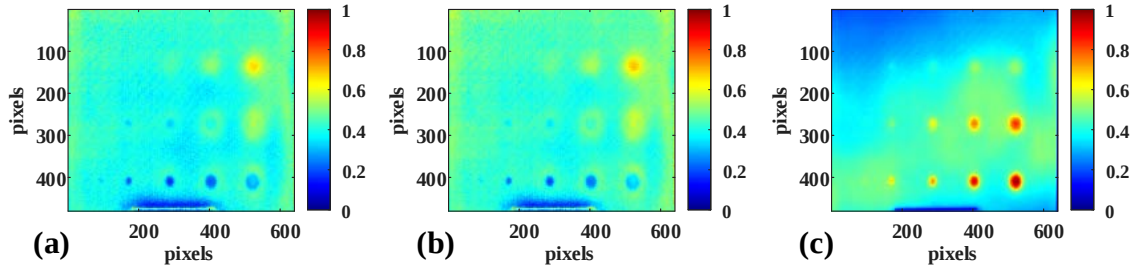

Figure 7. Results of total harmonic distortion method; (a) THD_P, (b) THD_A, (c) F_{Peak}

Compared with the THD method shown in Figure 7, it can be found that the effect of F_{Peak} treatment is better, and the detected defects are more obvious. Compared with the original image, part of the noise is filtered out, and the image quality is improved.

Evaluation of infrared image sequence processing algorithm

In order to compare the effects of different image sequence processing algorithms, as shown

in Figure 8, the rectangular area at the center of the debonding defect of CFRP laminates and the rectangular area without defects are selected to define the SNR for analysis. This implies that

$$SNR_p = \frac{\left|\overline{M_d} - \overline{M_{df}}\right|}{\sigma_p} \tag{15}$$

where SNR_p is the SNR of the image with the best contrast after processing by the image processing algorithm, $\overline{M_d}$ is the average pixel value corresponding to the defect area, $\overline{M_{df}}$ is the average pixel value corresponding to the defect-free region, and σ_p is the standard deviation of the pixel value corresponding to the defect-free area.

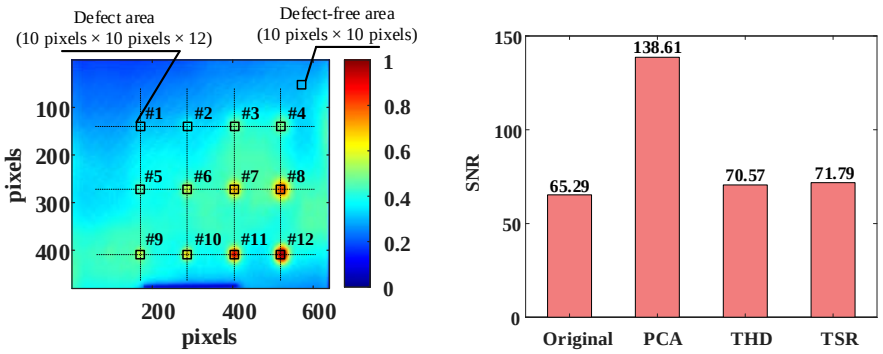

Figure 8. Signal-to-noise ratio reference areaFigure9. Calculation diagram of SNR

From Figure 9, it can be seen that, compared with the other two image sequence processing algorithms, PCA has stronger noise suppression ability, higher signal-to-noise ratio of processed images, more obvious defect edge display and stronger defect detection ability.

Conclusion

In order to detect debonding defects of CFRP laminates, a nonlinear frequency-modulated infrared thermal wave detection system was established. NLFM signal modulates the halogen lamp, and the halogen lamp emits energy light wave to generate temperature difference on the surface of CFRP laminates. Infrared thermography is used to collect surface temperature data of CFRP laminates. Aiming at the problem of noise interference in the collected heat map sequence, this paper adopts PCA, TSR and THD to process the image sequence. By calculating the SNR of the result images processed by the three algorithms, it can be seen that PCA has the highest SNR compared with the other two algorithms and can effectively improve the extraction of specimen defect information.

Acknowledgment

This project is supported by National Natural Science Foundation of China (Grant No. 51775175),Heilongjiang Provincial Undergraduate University Funded Project of Basic Scientific Research Business Fee(Grant No. 2020-KYYWF-0696), and Heilongjiang Province Natural Science Fund (Grant No. LH2021E088).

Nomenclature

T - modulation time, [s]

f_s - initial frequency, [Hz]

f_e - termination frequency, [Hz]

φ_0 - initial phase, [-]

Reference

[1] Qiu, C., *et al*., Research and Application Progresses of Thin-ply Carbon Fiber Reinforced Polymer Matrix Composites, *Aeronautical Manufacturing Technology*, 64 (2021), 14, pp. 22-31

[2] Yang, N. B., *et al*., Analysis on Composite Materials Used on Airframe Structure of Large Civil Aircraft, *Aeronautical Manufacturing Technology*, 5 (2009), 2, pp. 68-70

[3] Su, F., *et al*., Formation Mechanism of the Slotting Delamination of Carbon Fiber Reinforced Plastics,*Acta Materiae Compositae Sinica*, 38 (2021), 12, pp. 4042-4051

[4] Milne, J. M., *et al*., The Non-destructive Evaluation of Composites and Other Materials by Thermal Pulse Video Thermography, *Proceedings of the society of photo-optical instrumentation engineers*, 520 (1985), pp. 119-122

[5] Almond, D. P., *et al*., An Analytical Study of the Pulsed Thermography Defect Detection Limit, *Journal of Applied Physics*, 111 (2012), 9, pp. 093510

[6] Busse, G., *et al*., Thermal Wave Imaging with Phase Sensitive Modulated Thermography, *Journal of Applied Physics*, 71 (1992), 8, pp. 3962-3965

[7] Tabatabaei, N., *et al*., Thermal Coherence Tomography Using Match Filter Binary Phase Coded Diffusion Waves, *Physics Review Letters*,107 (2011), 16, pp. 165901

[8] Mulaveesala, R., *et al*., Complementary Coded Thermal Wave Imaging Scheme for Thermal Non-destructive Testing and Evaluation, *Quantitative Infrared Thermography Journal*, 14 (2017), 1, pp. 44-53

[9] Liu, J. Y., *et al*., Infrared Thermal Wave Imaging Detection Technology Excited by Linear Frequency Modulation, *Infrared and Laser Engineering*, 41 (2012), 6, pp. 1416-1422

[10] Saeid, H., *et al.*, On the Application of an Optimized Frequency-phase Modulated Waveform for Enhanced Infrared Thermal Wave Radar Imaging of Composites, *Optics and Lasers in Engineering*, 137 (2021), Mar., pp.106411

[11] Roche, J. M., *et al.*, Images of Thermographic Signal Reconstruction Coefficients: a Simple Way for Rapid and Efficient Detection of Discontinuities, *Materials evaluation*, 72 (2014), 1, pp. 73-82

[12] Rajic, N., *et al*., Principal Component Thermography for Flaw Contrast Enhancement and Flaw Depth Characterisation in Composite Structures, *Composite structures*, 58 (2002), 4, pp. 521-528

[13] Shmilovitz, D., *et al*., On the Definition of Total Harmonic Distortion and its Effect on Measurement Interpretation, *IEEE Transactions on Power delivery*, 20 (2005), 1, pp. 526-528

Paper submitted: August 9, 2022
Paper revised: November 15, 2022
Paper accepted: November 22, 2022